SGLI

Algorithm Technical Background Document

ATMOSPHERIC CORRECTION ALGORITHM FOR OCEAN COLOR

Version 1 Rev.1 January 17 2019

Mitsuhiro Toratani,
Kazunori Ogata and Hajime Fukushima
Tokai University

Version/Revision History:

V.1 Rev.1: January 17, 2019

Version 1	December 20, 2018	
V.1 Rev.1	January 17, 2019	Several mistakes corrected Contents page enhanced Cover page added Page numbers added Introduction section added

Table of Contents

1. Introduction to Version 1 Revision 1 Description

This document describes the atmospheric correction algorithm (Ver.1 Rev.1) for SGLI Level 2 standard ocean color product generation. The algorithm is to produce the normalized water-leaving radiance, or the upwelling radiance emitted from just beneath the sea surface (unit: $W/m^2/\mu m/sr$) for each relevant observation band. As a bi-product, the algorithm also produces aerosol optical thickness (AOT, dimensionless) for several near infrared bands.

The algorithm inherits its basic structure from the GLI ocean color atmospheric correction algorithm (Fukushima et al., 1998): Toratani et al., 2007), but some modifications and enhancements have been applied. One significant difference from the past algorithm is the selection of NIR band pair in terms of aerosol type/optical thickness determination: that is, lacking 750 nm band in SGLI channels, we use (673nm, 869nm) band pair with an iterative procedure to estimate Rrs (673). Another feature of atmospheric correction is the use of (865nm, 1630nm) band pair observation, in addition to (673nm, 869nm), to ensure the quality of aerosol reflectance estimation over turbid waters. The algorithm also incorporates BRDF correction.

2. Radiative transfer model

The satellite-observed radiance, L_T^*, is modeled as follows.

$$\boldsymbol{L_T^* = L_{path}^* + T^* L_G + t^* L_{(WC)} + t^* L_W [W\, m^{-2}\, \mu m^{-1}\, sr^{-1}]} \quad (2.1)$$

For simplicity, omit the wavelength (λ). L_{path}^* is radiance that contribution of the atmosphere composed of atmospheric scattered light and sea surface specular reflection of sky light, L_G is the radiance resulting from the specular reflection by the direct sun light, $L_{(WC)}$ is the radiance resulting from the whitecap, L_W is water-leaving radiance. T^* is the direct transmittance of the atmosphere from sea surface to satellite, t^* is the diffuse transmittance of the atmosphere from sea surface to satellite.

$T^*$and t^* are component as follows,

$$\boldsymbol{T^* = T^{(O3)} T^{(g)} T^{(M)} T^{(A)}} \quad (2.2)$$

$$\boldsymbol{t^* = t^{(O3)} t^{(g)} t^{(M)} t^{(A)}} \quad (2.3)$$

$t^{(O3)}$ is transmittance of ozone absorption, $t^{(g)}$ is transmittance of gas (O_2, NO_2, H_2O) absorption excluding ozone, $t^{(M)}$ is transmittance of molecule, $t^{(A)}$ is transmittance of aerosol.

The satellite-observed radiance excluding the influence of ozone transmittance $\boldsymbol{L_T}$ is expressed as follows.

$$\boldsymbol{L_T^* = \left(\frac{L_{path}^*}{t^{(O3)} t_0^{(O3)}} + \frac{T^*}{t^{(O3)} t_0^{(O3)}} L_G + \frac{t^*}{t^{(O3)} t_0^{(O3)}} L_{WC} + \frac{t^*}{t^{(O3)} t_0^{(O3)}} L_W \right) t^{(O3)} t_0^{(O3)}}$$

$$\boldsymbol{L_T^* = \left(L_{path} + T L_G + t L_{WC} + t L_W \right) t^{(O3)} t_0^{(O3)}}$$

$$\boldsymbol{L_T = L_{path} + T L_G + t L_{WC} + t L_W} \quad (2.4)$$

where the element without superscript * has the meaning of correcting the transmittance due to ozone. Since the ozone layer is in the upper atmosphere layer, the influence of ozone is corrected in advance.

L_{path} is represented by the following atmospheric radiances.

$$\boldsymbol{L_{path} = L_M + L_A + L_{MA}} \quad (2.5)$$

$L_M$is molecule radiance, L_A is aerosol radiance, L_{MA} is radiance due to the interaction between molecules and aerosol particles.

The Eq.(2.5) is substituted into Eq. (2.4).

$$\boldsymbol{L_T = L_M + L_A + L_{MA} + T L_G + t L_{WC} + t L_W} \quad (2.6)$$

3. Radiative transfer model for reflectance

In atmospheric correction processing, reflectance (ρ) is used. The relationship between reflectance and radiance(L) is as follows.,

$$\boldsymbol{\rho(\lambda) = \frac{\pi L(\lambda)}{F_0(\lambda)\cos\theta_0}}, \qquad (3.1)$$

where F_0 is Extraterestrial solar irradiance, θ_0 is solar zenith angle.

The extraterrestrial solar irradiance (F_0) depend on the distance between the sun and the earth. The relationship between F_0 and extraterrestrial solar irradiance ($\overline{F_0}$) at mean distance between solar and the earth is as follows.

$$F_0(\lambda) = \overline{F_0}(\lambda) \cdot daycor^2$$

$$daycor = \frac{1}{1.00014 - 0.01671 * \cos\alpha - 0.00014 * cos^2 2\alpha}$$

$$\alpha = 0.9856002831 * jday - 3.4532868 \quad \text{(degree)}$$

jday : day of year.

For mean extraterrestrial solar irradiance, see Appendix I.

By substituting this expression, the Eq. (2.6) becomes as follows.

$$\boldsymbol{L_T = L_M + L_A + L_{MA} + TL_G + tL_{WC} + tL_W}$$

$$\boldsymbol{\frac{\pi L_T}{F_0\cos\theta_0} = \frac{\pi(L_M + L_A + L_{MA} + L_G + tL_{WC} + tL_W)}{F_0\cos\theta_0}}$$

$$\boldsymbol{\rho_T = \rho_M + \rho_A + \rho_{MA} + T\rho_G + t\rho_{WC} + t\rho_w} \qquad (3.2)$$

$$\boldsymbol{\rho_w = \frac{\rho_T - (\rho_M + \rho_A + \rho_{MA} + T\rho_G + t\rho_{WC})}{t}} \qquad (3.3)$$

The ρ_w is calculated by subtracting ρ_M, $\rho_A + \rho_{AM}$, $T\rho_G$, $t\rho_{WC}$ and dividing by t.
The $\rho_{(rc)}$ used for cloud detection is defined as

$$\boldsymbol{\rho_{(rc)} = \rho_T - \rho_M}$$

4. Overview of atmospheric correction for SGLI

The flowchart of atmospheric correction for SGLI shows in fig.4.1. Processing of each pixel is executed in the order of Ozone transmittance, Rayleigh reflectance, Cloud screening, Sunglitter, Whitecap, Aerosol reflectance, and bidirectinal reflectance distribution function to estimate water-leaving radiance (nLw) from Satellite-observed radiance (Lt).

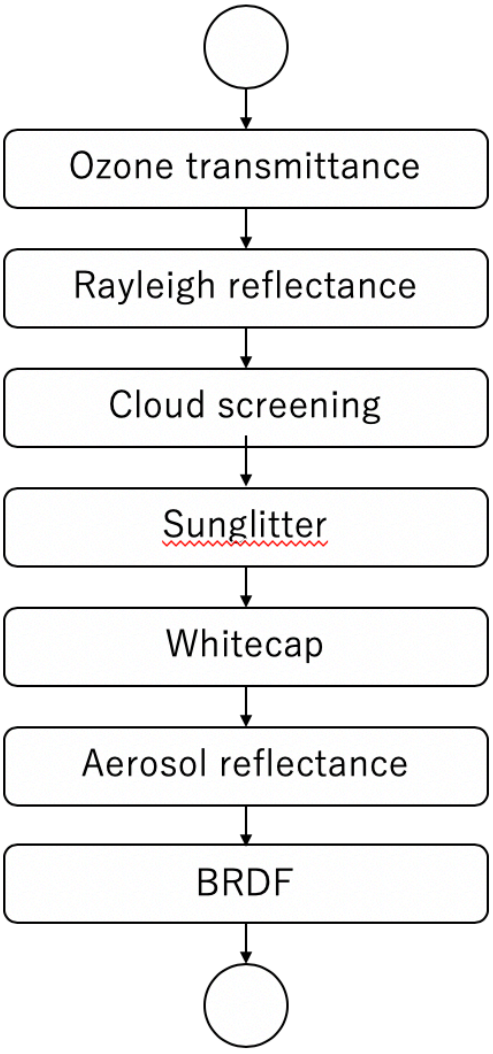

Fig. 4.1 Flowchart of atmospheric correction for SGLI

Correction of ozone transmittance is attenuation due to absorption of ozone (Chapter 7, Section 2). Rayleigh reflectance correction is correction of scattering of gas molecules (Chapter 5). Pixels above the threshold ($\rho_{(rc)}(865) = 0.03$) are masked as clouds. The sunglint reflectance is corrected by the method of Cox & Munk (Chapter 8). The white cap correction is described in Chapter 9. The most complicated part of atmospheric correction is correction of reflectance of aerosol. In order to calculate the

aerosol reflectance, two aerosol models are selected from prepared aerosol models. In the aerosol model selection, the near infrared region is usually used for selecting the aerosol model, but in the case of the influence of the high suspended matter concentration, the short wavelength infrared region is used. In the case of aerosol model selection using the near infrared region, iteration procedure is used to avoid contribution of water-leaving reflectance at near infrared bands. Details are shown in Chapter 6. Correction of bidirectinal reflectance distribution function described in Chapter 10. In this chapter, the definition of normalized water-leaving radiance is also described.

5. Rayleigh reflectance (ρ_M)

The reflectance due to the scattering by atmospheric molecule, $\rho_M(\lambda)$, is calculated by using lookup tables. The lookup tables give $\rho_M(\lambda)$ for the given $\theta(\lambda)$, θ_0 and $\Delta\phi$. The lookup tables have 24 values for satellite zenith angle in 3.5° increments (0.0° - 80.5°) and 24 values for solar zenith angle in 3.5° increments (0.0° - 80.5°). If there is no exact values for the target pixel in the lookup table the values needed are interpolated by two-dimensional linear interpolation.

The lookup tables were constructed by solving the Radiative Transfer Model at standard atmospheric pressure and the absorption of ozone layer was not taken into account. At this stage, we correct the pressure impact with aid of the pressure ancillary data.

$\rho_M(\lambda)$ in consideration of pressure impact is calculated by the following equation:

$$\rho_M(\lambda) = \frac{1 - exp\left(-\tau_M(\lambda)/cos\theta(\lambda)\right)}{1 - exp\left(-\tau_{M0}(\lambda)/cos\theta(\lambda)\right)} \rho_{M0}(\lambda, \theta(\lambda), \theta_0, \Delta\phi) \qquad (5.1)$$

τ_M: Rayleigh optical thickness

τ_{M0}: Rayleigh optical thickness at standard atmospheric pressure. τ_{M0} at each band is shown below.

θ: zenith angle of the satellite

θ_0: zenith angle of the sun

ρ_{M0}: Rayleigh reflectance which are calculated from lookup tables

$\Delta\phi$: difference between the solar and the satellite azimuth angles

The Rayleigh optical thickness, τ_M, is calculated by the following equations:

$$\tau_M(\lambda) = \frac{P}{P_0} \tau_{M0}(\lambda) \qquad (5.2)$$

P: atmospheric pressure at each pixel.

P_0: standard atmospheric pressure (= 1013.25hPa)

$\tau_{M0}(\lambda)$: Rayleigh optical thickness at standard atmospheric pressure. τ_{M0} at each band was computed by the following equation (Bodhaine, 1999) in consideration with sensor response function.

$$\tau_{r0}(\lambda) = 0.0021520 \left(\frac{1.0455996 - 341.29061\lambda^{-2} - 0.90230850\lambda^2}{1 + 0.0027059889\lambda^{-2} - 85.968563\lambda^2} \right) \qquad (5.3)$$

λ : wavelength(μm)

Table 5.1 Rayleigh optical thickness at standard atmospheric pressure in consideration with sensor response function

Band	Rayleigh optical thickness	Band	Rayleigh optical thickness
VN1	0.4467	VN9	0.02571
VN2	0.3189	VN10	0.01525
VN3	0.2361	VN11	0.01525
VN4	0.1559	SW1	0.007107
VN5	0.1132	SW2	0.002380
VN6	0.08714	SW3	0.001246
VN7	0.04265	SW4	0.0003765
VN8	0.04265		

5.1 Lookup tables for the reflectance due to Rayleigh scattering

The lookup table of each band gives $\rho_M(\lambda)$ for 3 parameters, i.e., $\theta(\lambda)$, θ_0 and $\Delta\phi$.

(1) Calculation

The tables were calculated for the following values of the independent variables and conditions:

- θ : 0.0° - 80.5°(24 points)
- θ_0 : 0.0° - 80.5° in 3.5° increments(24 points)
- $\Delta\phi$: 0.0° - 180° in 4.0° increments(46 points)
- Atmospheric pressure : standard atmospheric pressure(1013.25hPa)
- The polarization was considered.
- The absorption of ozone layer was ignored.
- The multiple scattering due to the interaction between molecules was considered.
- The sea surface was assumed to be flat.
- A plane parallel atmosphere divided into several homogeneous sublayers was assumed.
- Reflectance due to sun glint was removed.
- Response function was considered.

The lookup table are constructed by radiative transfer code (pstar4 : Ohta et al.,2008).

6. Aerosol reflectance ($\rho_A + \rho_{MA}$)

6.1. Overview

The spectral variation in ρ_T in the near infrared is used to provide information concerning the aerosol's optical properties. The Rayleigh-scattering component is then removed, and the spectral variation of the remainder is compared with that produced by a set of candidate aerosol models in order to determine which two models of the candidate set are most appropriate. We implemented tables that store the relationship between aerosol reflectance $\rho_A + \rho_{MA}$ and aerosol optical thickness τ_A for each band. The magnitude of $\rho_A + \rho_{MA}$ in the shorter wavelength bands is estimated from the spectral ratio of aerosol reflectance between two near infrared bands. Since the spectral dependency of $\rho_A + \rho_{MA}$ is dependent on aerosol type.

Generally, we use near infrared bands for aerosol model selection. If there are high suspended matter, we use shortwave infrared bands to avoid water contribution. Just by changing the near infrared bands to shortwave infrared bands, the method of aerosol model selection does not change without iteration.

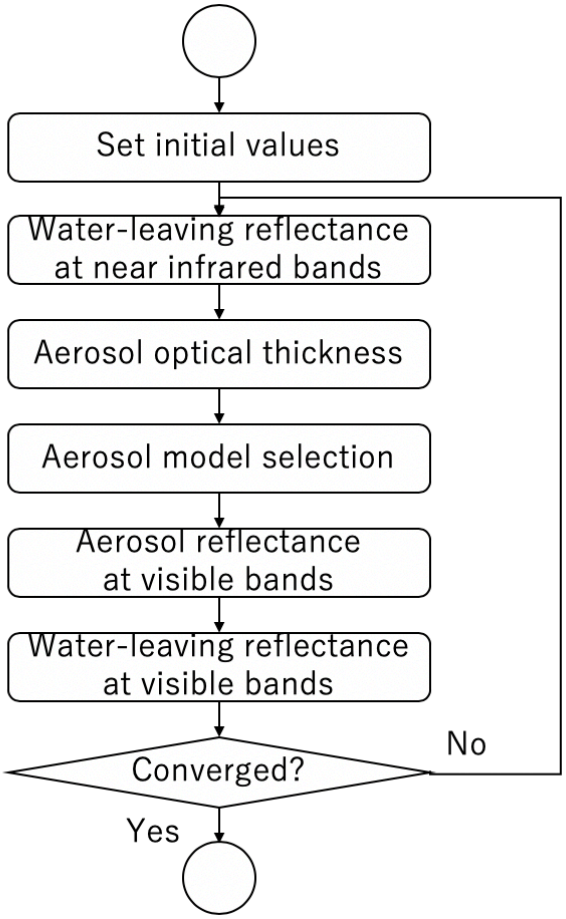

Figure 6.1 Flowchart of aerosol reflectance correction using iteration

Flowchart of aerosol reflectance estimation is shown in Fig.6.1. Water-leaving reflectance is estimated using initial values (Chlorophyll-a concentration, and CDOM). $\rho_A(\lambda_S) + \rho_{MA}(\lambda_S)$ and $\rho_A(\lambda_l) + \rho_{MA}(\lambda_l)$ ($\lambda_S = 670$, $\lambda_l = 865$ at near infrared bands, $\lambda_S = 865$, $\lambda_l = 1630$ in case of high turbid.) are converted to aerosol optical thickness (τ_A) using lookup tables (Section 6.4) of relationship between $\rho_A + \rho_{MA}$ and τ_A for aerosol models. Aerosol models are selected from the spectral dependency of τ_A. $\rho_A + \rho_{MA}$ in the visible bands is estimated using the selected aerosol models.

After the first atmospheric correction, the new water-leaving reflectance is estimated from the obtained CHL and CDOM, with atmospheric correction repeated until these values converged. We set the threshold for the convergence condition as the stage at which the difference in CHL between, before and after processing was less than 1% and the difference in CDOM was less than 0.001 m^{-1}. A total of ten iterations were performed.

The algorithm is switched in case of high turbid water or not. We use $\lambda_S = 670$, $\lambda_l = 865$ at near infrared bands for Case I water, $\lambda_S = 865$, $\lambda_l = 1630$ for high turbid water. The switching is explained in Section 6.2.

Regarding correction of absorptive aerosol, it was postponed.

6.2 Switching process in consideration to high turbid water

In considering the influence of suspended matter concentration, it is divided into three regions, Case 1, Case 2 and its transition area. We call NIR-AC for Case 1 atmospheric correction, SWIR-AC for Case 2 atmospheric correction.
T-index was used for division.

$$T_{ind}(869,1630) = \frac{\rho_{(rc)}(673)}{\rho_{(rc)}(869)} \exp\left\{-\frac{869-673}{1630-869} ln\left(\frac{\rho_{(rc)}(869)}{\rho_{(rc)}(1630)}\right)\right\}. \quad (6.1)$$

NIR-AC method is used if T_{ind} is less than th_{low}, and SWIR-AC method is used if T_{ind} is greater than th. If T_{ind} includes between th_{low} and th then $\rho_A + \rho_{MA}$ is estimated by liner interpolation between NIR-AC and SWIR-AC methods (Figure 6.2).

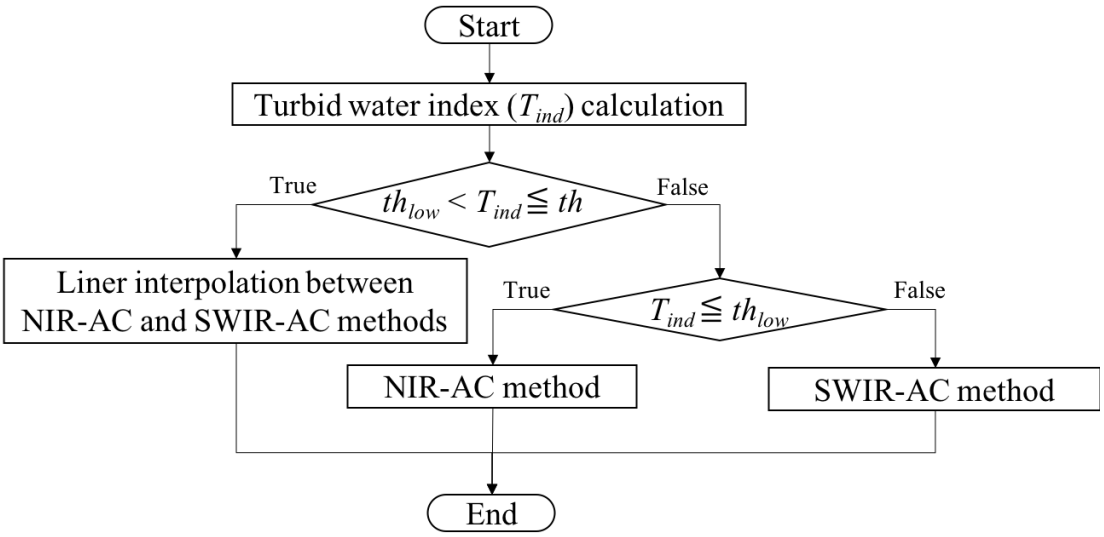

Figure 6.2 Method of switching Case 1, Case 2 and its transition

6.3 Determination of aerosol type from near infrared bands

$\rho_A(\lambda_S) + \rho_{MA}(\lambda_S)$ and $\rho_A(\lambda_l) + \rho_{MA}(\lambda_l)$ ($\lambda_S = 670$, $\lambda_l = 865$ at near infrared bands) are calculated by the following equation where $\rho_W(\lambda)$ is calculated by using in-water model.

$$\rho_A(\lambda) + \rho_{MA}(\lambda) = \rho_T(\lambda) - \rho_M(\lambda) - t(\lambda)\,\rho_G(\lambda) - t(\lambda)\,\rho_W(\lambda) \quad (6.2)$$

Then $\tau_A(M, \lambda_S)$ and $\tau_A(M, \lambda_l)$ are obtained by following equation.

$$X = \rho_A(M,\lambda,\theta,\theta_0,\Delta\phi) + \rho_{MA}(M,\lambda,\theta,\theta_0,\Delta\phi)$$

$$\tau_A(M,\lambda,\theta,\theta_0,\Delta\phi) = a_0 + a_1X + a_2X^2 + a_3X^3 + a_4X^4 \quad (6.3)$$

M: aerosol model

λ: wavelength

θ: a zenith angle of the satellite

θ_0: a zenith angle of the sun

$\Delta\phi$: a difference between the solar and the satellite azimuth angles

a_0, a_1, a_2, a_3 and a_4: These values are provided by the lookup tables.

The pixel-wise procedure for the atmospheric correction is described as follows. In what follows, $\varepsilon'(M)$ means the estimated value of the spectral ratio of $\omega_A\tau_A P_A$ between 670 and 865nm bands for an assumed aerosol model M, while $\varepsilon(M)$ is the theoretically derived value of $\omega_A K_{EXT} P_A$ ratio for a model M.

(1) Get $\rho_A(\lambda) + \rho_{MA}(\lambda) = \rho_T(\lambda) - \rho_M(\lambda)$ at 670 and 865nm.

(2) Estimate τ_A at 670nm and 865nm bands for each assumed aerosol model(M) by solving the biquadratic equation in reference to the aerosol LUTs (LookUp Table).

(3) Calculate ε'_{ave} and select a pair of aerosol models A and B, such that $\varepsilon(A) < \varepsilon'_{ave}$ and

$\varepsilon(B) > \varepsilon'_{ave}$, by the iteration scheme. Define interpolation ratio r as $(\varepsilon'_{ave} - \varepsilon(A))/(\varepsilon(B) - \varepsilon'(A))$.

(4) For models A and B, obtain $\tau_A(\lambda,M)$ for band 380nm to 565nm by

$$\tau_A(\lambda,M) = \frac{K_{ext}(\lambda,M)}{K_{ext}(865,M)}\tau_A(865,M) \tag{6.4}$$

Derive $\rho_A(\lambda)+\rho_{MA}(\lambda)$ for the models A and B in use of the aerosol LUT.

(5) Obtain final $\rho_A(\lambda)+\rho_{MA}(\lambda)$ by interpolating the $\rho_A+\rho_{MA}$ values for the models A and B.

6.4 Determination of aerosol type from shortwave infrared bands

$\rho_A(\lambda_S) + \rho_{MA}(\lambda_S)$ and $\rho_A(\lambda_l) + \rho_{MA}(\lambda_l)$ ($\lambda_S = 865$, $\lambda_l = 1630$ in case of high turbid.) are calculated by the same equation (6.2) as $\rho_W(1630)=0$. SWIR-AC method estimates $\rho_A(\lambda)+ \rho_{MA}(\lambda)$ in the basis of the single scattering approximation using $\rho_{(rc)}(865)$ and $\rho_{(rc)}(1630)$ pair. In contrast to NIR-AC, this method doesn't use the iterative procedure using the in-water model. The reason why is that the contribution of water-leaving reflectance for wavelengths longer than visible can be ignored because of having strongly light absorption on water property of these wavelengths.

The Outline of SWIR-AC method is described as follows. In what follows, ε'(M) means the estimated value of the spectral ratio of $\omega_A\tau_A P_A$ between 865nm and 1630nm channels for an assumed aerosol model M, while ε(M) is the theoretically derived value of $\omega_A K_{EXT} P_A$ ratio for a model M.

(1) Get $\rho_A(\lambda)+ \rho_{MA}(\lambda)= \rho_T(\lambda)-\rho_M(\lambda)$ at 865nm and 1630nm.

(2) Estimate τ_A at 865nm and 1630nm bands for each assumed aerosol model(M) by solving the biquadratic equation in reference to the aerosol LUTs.

(3) Calculate ε'_{ave} and select a pair of aerosol models A and B, such that $\varepsilon(A) < \varepsilon'_{ave}$ and $\varepsilon(B) > \varepsilon'_{ave}$, by the iteration scheme. Define interpolation ratio r as $(\varepsilon'_{ave} - \varepsilon(A))/(\varepsilon(B) - \varepsilon'(A))$.

(4) For models A and B, obtain $\tau_A(\lambda,M)$ for band 380nm to 670nm by

$$\tau_A(\lambda,M) = \frac{K_{ext}(\lambda,M)}{K_{ext}(1630,M)}\tau_A(1630,M). \tag{6.5}$$

Derive $\rho_A(\lambda)+\rho_{MA}(\lambda)$ for the models A and B in use of the aerosol LUT.

(5) Obtain final $\rho_A(\lambda)+\rho_{MA}(\lambda)$ by interpolating the $\rho_A+\rho_{MA}$ values for the models A and B.

6.5 Liner interpolation between NIR-AC and SWIR-AC methods

$\rho_A(\lambda)+ \rho_{MA}(\lambda)$ and τ_A is calculated by both of NIR-AC and SWIR-AC method if the T_{ind} includes between th_{low} and th. In this case, desiring parameters, p_d, are represented by liner interpolation using weight calculated from the T_{ind} as follows,

$$p_d = wp_n + (1-w)p_s$$
$$w = \frac{th - T_{ind}(869,1630)}{th - th_{low}} \quad (6.6)$$

where p_n is the parameter estimated by NIR-AC method and p_s is the parameter estimated by SWIR-AC method.

6.6 Lookup tables for the reflectance due to aerosol scattering

The lookup table of each NIR band and aerosol model contains coefficients a_0, a_1, a_2, a_3 and a_4 of the following equation.

$$X = \rho_A(M,\lambda,\theta,\theta_0,\Delta\phi) + \rho_{MA}(M,\lambda,\theta,\theta_0,\Delta\phi)$$
$$\tau_A(M,\lambda,\theta,\theta_0,\Delta\phi) = a_0 + a_1X + a_2X^2 + a_3X^3 + a_4X^4 \quad (6.7)$$

M: aerosol model
θ: a zenith angle of the satellite
θ_0: a zenith angle of the sun
Δϕ: a difference between the solar and the satellite azimuth angles

On the other hand, the lookup table of each visible band and aerosol model contains coefficients b_0, b_1, b_2, b_3 and a_4 of the following equation.

$$X = \tau_A(M,\lambda,\theta,\theta_0,\Delta\phi)$$
$$\rho_A(M,\lambda,\theta,\theta_0,\Delta\phi) + \rho_{MA}(M,\lambda,\theta,\theta_0,\Delta\phi) = b_0 + b_1X + b_2X^2 + b_3X^3 + b_4X^4 \quad (6.8)$$

M: aerosol model
θ: a zenith angle of the satellite
θ_0: a zenith angle of the sun
Δϕ: a difference between the solar and the satellite azimuth angles

6.6.1 Calculation

The tables were calculated for the following values of the independent variables and conditions:

– θ and θ_0 : 0.0° - 80.5° in 3.5° increments
– ΔΦ : 0.0° - 180.0° in 4° increments
– τ_A : 0.01, 0.02, 0.03, 0.07, 0.1, 0.2, 0.3
– Atmospheric pressure : standard atmospheric pressure(1013.25hPa)
– The polarization was considered.
– The absorption of ozone layer was ignored.
– The multiple scattering due to the interaction between molecules and aerosol particles was considered.

– The sea surface was assumed to be flat.
– A plane parallel atmosphere divided into 50 homogeneous sublayers was assumed.
– Reflectance due to sun glint was removed.
– Response function was considered.
– aerosol models :

Table 6.1 Aerosol models

	Aerosol volume ration		Relative Humidity (%)
	Tropospheric	Oceanic	
Model1	1	0	70
Model2	1	0.32	70
Model3	1	0.64	70
Model4	1	1.28	70
Model5	1	2.56	60
Model6	1	2.56	73
Model7	1	5.14	70
Model8	1	10.39	70
Model9	0	1	83

The lookup table are constructed by radiative transfer code (pstar4 : Ohta et al.,2008).

6.6.2 Interpolation

It uses Lagrange's interpolation for sun and satellite zenith angles and azimuth angle difference which are not covered in the tables. When 60°≥θ and 60°≥θ_0 one degree Lagrange's interpolation is used to obtain a_n. And when θ>60° or θ_0>60° two degree Lagrange's interpolation is used.

(1) Calculation formula for one degree Lagrange's interpolation (when 60°≥θ and 60°≥θ_0)

$$a_n(\theta,\theta_0,\Delta\phi)=\sum_{i=u}^{u+1}\sum_{j=v}^{v+1}\sum_{k=w}^{w+1}A_{n,ijk}\cdot L_i(\theta)\cdot M_j(\theta_0)\cdot N_k(\Delta\phi) \tag{6.9}$$

The condition of the grid point numbers, *u, v* and *w,* are as follows.

$u<\theta<u+1$

$v<\theta_0<v+1$

$w<\Delta\phi<w+1$

where

$0\le u\le 22,\ 0\le v\le 22,\ 0\le w\le 44$

$A_{n,ijk}$: values in grid points i, j, k. It's obtained from the lookup table.

θ: the zenith angle of the satellite. 0 - 80.5°, 3.5° increments, 24 data, i = 0,....., 23

θ_0: the zenith angle of the sun. 0 - 80.5°, 3.5° increments, 24 data, j = 0,....., 23

$\Delta\phi$: the difference between the solar and the satellite azimuth angles. 0 - 180.0° , 4.0° increments, 46 data, k = 0,....., 45

$$L_u(\theta) = \frac{(\theta - \theta_{u+1})}{(\theta_u - \theta_{u+1})}$$
$$L_{u+1}(\theta) = \frac{(\theta - \theta_u)}{(\theta_{u+1} - \theta_u)} \qquad (6.10)$$

The shape of equations $M_j(\theta_0)$ and $N_k(\Delta\phi)$ are the same as those of $L_i(\theta)$.

(2) Calculation formula for two degree Lagrange's interpolation (when θ>60° or θ_0>60°)

$$a_n(\theta,\theta_0,\Delta\phi) = \sum_{i=u}^{u+2}\sum_{j=v}^{v+2}\sum_{k=w}^{w+2} A_{n,ijk} \cdot L_i(\theta) \cdot M_j(\theta_0) \cdot N_k(\Delta\phi) \qquad (6.11)$$

u+1, v+1, w+1 : grid points closest to $\theta, \theta_0, \Delta\phi$

where

$0 \le u \le 21$, $0 \le v \le 21$, $0 \le w \le 43$

$A_{n,ijk}$: values at grid point i, j, k. It's obtained from the lookup table.

θ: the zenith angle of the satellite. 0 - 80.5°, 3.5° increments, 24 data, i = 0,....., 23

θ_0: the zenith angle of the sun. 0 - 80.5°, 3.5° increments, 24 data, j = 0,....., 23

$\Delta\phi$: the difference between the solar and the satellite azimuth angles. 0 - 180.0°, 4.0° increments, 46 data, k = 0,....., 45

$$L_u(\theta) = \frac{(\theta - \theta_{u+1})(\theta - \theta_{u+2})}{(\theta_u - \theta_{u+1})(\theta_u - \theta_{u+2})}$$
$$L_{u+1}(\theta) = \frac{(\theta - \theta_u)(\theta - \theta_{u+2})}{(\theta_{u+1} - \theta_u)(\theta_{u+1} - \theta_{u+2})}$$
$$L_{u+2}(\theta) = \frac{(\theta - \theta_u)(\theta - \theta_{u+1})}{(\theta_{u+2} - \theta_u)(\theta_{u+2} - \theta_{u+1})} \qquad (6.12)$$

The shape of equations $M_j(\theta_0)$ and $N_k(\Delta\phi)$ are the same as those of $L_i(\theta)$.

7. Transmittence

7.1 Moleculer transmittance

The moleculer transmittance is obtained by following equation.

$$t_M(\lambda) = \exp\left(-\frac{\tau_M(\lambda)}{2\cos x}\right) \qquad (7.1)$$

x : θ (λ) or θ_0

$\tau_M(\lambda)$: molecular optical thickness is described in section 3.

7.2 Ozone absorption correction

The ozone transmittance is obtained by following equation.

$$t_{OZ}(\lambda) = \exp\left\{\frac{-\tau_{OZ}(\lambda)}{\cos x}\right\} \qquad (7.2)$$

x : θ (λ) or θ_0

$\tau_{OZ}(\lambda)$: optical thickness of ozone

$$\tau_{OZ}(\lambda) = DU \cdot K_{OZ}(\lambda) \qquad (7.3)$$

$K_{OZ}(\lambda)$: coefficients which relate optical thickness of ozone and DU.

K_{OZ} is calculated beforehand (Table 7.1)

DU : Total ozone. DU(Dobson Unit) means total ozone concentration at 0°C, 1hPa (above mean sea level) and one DU is equal to a hundredth of the ozone layer thickness. DU at each band is shown below.

Table 7.1 Coefficients which relate optical thickness of ozone and DU in consideration with sensor response function

Band	$<K_{oz}(\lambda)>[DU^{-1}]$	Band	$<K_{oz}(\lambda)>[DU^{-1}]$
VN1	7.97e-08	VN9	7.59e-06
VN2	4.33e-07	VN10	2.10e-08
VN3	3.74e-06	VN11	2.10e-08
VN4	2.25e-05	SW1	0.00e+00
VN5	6.79e-05	SW2	0.00e+00
VN6	1.17e-04	SW3	0.00e+00
VN7	4.42e-05	SW4	0.00e+00
VN8	4.42e-05		

7.3 Oxygen absorption correction

The O_2 A-band absorption usually reduces more than 10–15% of the measured radiance at the SGLI 763nm band. Ding and Gordon (1995) proposed a numerical

scheme to remove the O_2 A-band absorption effects on the SeaWiFS atmospheric correction.

$$t_{OZ}(763) = \frac{1}{1+10^{a+b\cdot M+cM^2}} \qquad (3\text{-}5)$$

where

M : airmass

a = 21.3491, b = 10.1155, and c = 27.0218 3x 10^{-3}.

8. Sunglitter correction

Reflectance of sun glint is calculated by following equations.

$$\boldsymbol{\rho_g(\lambda) = \frac{\pi f(\omega,\lambda) P_W(\theta,\theta_0,\Delta\phi,W)}{4 \cdot \cos\theta \cdot \cos\theta_0 \cdot \cos^4\theta_n}} \qquad (\mathbf{8}.1)$$

where

$P_W(\theta,\theta_0,\Delta\phi,W)$: probability of seeing sun

$$P_W(\theta,\theta_0,\phi,\phi_0,W) = \frac{1}{\pi\sigma^2}\exp\left(\frac{-\tan^2\theta_n}{\sigma^2}\right) \qquad (8.2)$$

$$\sigma^2 = 0.003 + 0.00512W.$$

$$\theta_n = \cos^{-1}\left(\frac{\cos\theta + \cos\theta_0}{2\cos\omega}\right) \qquad (8.3)$$

$$\cos 2\omega = \cos\theta\cos\theta_0 + \sin\theta\sin\theta_0\cos(\phi - \phi_0).$$

θ,ϕ : satellite zenith and azimuth angle at typical band

θ_0,ϕ_0 : solar zenith and azimuth angle at typical band

W : wind speed (m/s)

λ : wavelength

$f(\lambda)$: Fresnel reflectance

$$f(\omega,\lambda) = 1 - (2 \cdot n \cdot y \cdot z) \cdot \cos\omega$$

$n(\lambda)$: refractive index

ω : incident angle

$$y = \sqrt{n(\lambda)^2 + \cos^2\omega - 1}/n$$

$$z = \frac{1}{\{\cos\omega + y \cdot n(\lambda)\}^2} + \frac{1}{\{y + n(\lambda)\cos\omega\}^2}.$$

When $\rho_g(\lambda) \geq 0.02$, the pixel is masked as sun glint.

9. Whitecap correction

The estimation of whitecap reflectance follows the form

$$\boldsymbol{L_{(WC)}(\lambda) = t(\lambda) \cdot t_0(\lambda) \cdot c(\lambda) \cdot R_{WC} \cdot W} \qquad (\mathbf{9}.1)$$

where c(λ) is wavelength dependent factor (Frouin et al., 1996) in table 9.1.
The Koepke effective reflectance for whitecaps (Rwc) is 0.22. W is whitecap coverage.
W depend on wind speed. It was explained by Stramska and Petelski(2003).

$$W = 8.75 \times 10^{-5} \ (U_{10} - 6.33)^3,$$

where U10 is 10m wind speed. Minimum wind speed is 6.33 m/s.

Table 9.1 Wavelength dependent factor

Band	c(λ)	Band	c(λ)
VN1	1.0	VN9	0.762766
VN2	1.0	VN10	0.640922
VN3	1.0	VN11	0.640922
VN4	1.0	SW1	0.526908
VN5	1.0	SW2	0.319608
VN6	0.990367	SW3	0.156282
VN7	0.884466	SW4	0.0
VN8	0.884466		

10. Bidirectional reflectance distribution function

The water-leaving radiance was defined as following (Morel and Gentili1996),

$$\boldsymbol{L_W(\theta.\theta_0,\Delta\phi) = E_d(0^+)\left\{\frac{(1-\bar{\rho})[1-\rho(\theta',\theta)]}{\left(1-\bar{r}R(\theta_0)\right)n^2}\right\}\frac{R(\theta_0)}{Q(\theta',\theta_0,\Delta\phi)}} \quad (10.1)$$

$\boldsymbol{n}$ ：Refractive index of sea water

$\boldsymbol{E_d(0^+)}$ ：Downward irradiance just above ocean surface

$\boldsymbol{(1-\bar{\rho})}$ ：The rate at which downward irradiance passes through the sea surface and enters the water

$\boldsymbol{[1-\rho(\theta',\theta)]}$ ：The rate at which the upward light underwater passes through the sea surface and passes through the air

$\frac{1}{1-\bar{r}R(\theta_0)}$ ：Multiple scattering at sea surface

Its Maclaurin's expansion is

$$1+\bar{r}R(\theta_0)+[\bar{r}R(\theta_0)]^2+[\bar{r}R(\theta_0)]^3+[\bar{r}R(\theta_0)]^4+\cdots\cdots$$

$R(\theta_0)$ ：Correction term when assuming that the sun is zenith.

$Q(\theta',\theta_0,\Delta\phi)$ ：the ratio between downward irradiance and upward radiance at just below surface

$$\boldsymbol{Q(\theta',\theta_0,\Delta\phi)=\frac{E_u(0^-)}{L_u(\theta',\theta_0,\Delta\phi)}} \quad (\mathbf{10}.2)$$

Eq.(10.1) is deformation of formula.

$$\boldsymbol{L_W(\theta.\theta_0,\Delta\phi) = [F_0\varepsilon t_0(\theta_0)\mu_0]\Re(\theta_0)\frac{R(\theta_0)}{Q(\theta',\theta_0,\Delta\phi)}} \quad (\mathbf{10}.3)$$

where

$$E_d(0^+) = F_0\varepsilon t_0(\theta_0)\mu_0$$

$$\Re(\theta) = \left\{\frac{(1-\bar{\rho})[1-\rho(\theta',\theta)]}{\left(1-\bar{r}R(\theta)\right)n^2}\right\}$$

F_0 ：mean extraterrestrial solar irradiance

ε ：Correction coefficient of sun-earth distance

$t_0(\theta_0)$ ：Defuse transmittance from space to sea surface

μ_0 ：$cos(\theta_0)$

nL_W is the water-leaving radiance in the zenith direction when the solar zenith angle is 0. nL_W is described using $\Re_0, Q_0, R_0$.

$$nL_W = \frac{F_0\Re_0}{Q_0}R_0$$

Using $\Re_0, Q_0, R_0$, the relational expression of L_W and nL_W is described as

$$\boldsymbol{L_W(\theta.\theta_0,\Delta\phi)=[\varepsilon t_0(\theta_0)\mu_0]\frac{R(\theta_0)}{R_0}\frac{\Re(\theta_0)}{\Re_0}\frac{Q_0}{Q(\theta',\theta_0,\Delta\phi)}nL_W} \quad (10.4)$$

There are three normalized water-leaving radiance, $(L_W)_N^S$ estimated from satellite observation data, $(L_W)_N^f$ by field observation, and exact normalized water-leaving radiance $(L_W)_N^{EX}$. Their relationship is as follows (Morel and Gentili, 1996; Appendix A).

$$\begin{aligned}(\boldsymbol{L_W})_N^{EX} &= \frac{\Re_0}{\Re(\theta)}\frac{R_0}{R(\theta_0)}\frac{Q(\theta',\theta_0,\Delta\phi)}{Q_0}(L_W)_N^S \\ &= \frac{R_0}{R(\theta_0)}\frac{Q(\theta_0)}{Q_0}(L_W)_N^f \end{aligned} \quad (10.5)$$

$R_{RS}$is defined

$$R_{RS}=\frac{L_W(\theta=0,\theta_0)}{E_d(0^+,\theta_0)}$$

The relationship between R_{RS} and nL_Ws (Morel and Gentili, 1996; Appendix B) is as follows.

$$R_{RS}=\frac{\Re_0}{Q(\theta_0)}R=\frac{(L_W)_N^f}{F_0}$$

$$R_{RS}=(L_W)_N^{EX}\frac{Q_0}{Q(\theta_0)}\frac{R(\theta_0)}{R_0}\frac{1}{F_0}$$

As a BRDF implementation for satellite ocean color data processing, we use Eq.(10.5). The correction factor of BRDF is calculated as the product of ratios of three coefficients.

The calculation of $\frac{\Re_0}{\Re(\theta)}\frac{R_0}{R(\theta_0)}$ consists of ratio of transmittance from in-water to air (t_{uf}) and transmittance from air to in-water (t_{df}) through the sea surface.

$$\frac{\Re_0}{\Re(\theta)}\frac{R_0}{R(\theta_0)}\frac{Q(\theta',\theta_0,\Delta\phi)}{Q_0}=\frac{t_{uf}(n,0)}{t_{uf}(n,\theta)}\frac{t_{df}(\lambda,0,0)}{t_{df}(\lambda,\theta_0,WS)}\frac{Q(\theta',\theta_0,\Delta\phi)}{Q(0,0)}$$

t_{uf} is function of reflactive index (n) and satellite zenith angle (θ), t_{df} is function of wavelength (λ), solar zenith angle (θ_0) and wind speed (WS).

10.1 Calculation of transmittance from in-water to air for satellite view (t_{uf})

t_{uf} is the Fresnel transmittance. The Fresnel transmittance has the following relationship with the Fresnel reflectance $(r_{uf}(n,\theta))$

$$t_{uf}(n,\theta)=1-r_{uf}(n,\theta)$$

10.2 Calculation of transmittance from air to in-water for solar path (t_{df})

$t_{df}(\lambda,\theta_0,WS)$ is calculated using following equation.

$$t_{df}(\lambda,\theta_0,WS)=1+c_1x+c_2x^2+c_3x^3+c_4x^4$$

where

$$x = \log(\cos\theta_0)$$

The coefficients c_1, c_2, c_3, c_4 depend on the wavelength (λ) and the wind speed (WS) in table 10.1.

Table 10.1 Coefficients c_1, c_2, c_3, c_4 from Wang (2006)

Wind speed (m/s)		Coefficents					
	Wavelength (nm)	412	443	490	510	555	670
0	c_1	-0.0087	-0.0122	-0.0156	-0.0163	-0.0172	-0.0172
	c_2	0.0638,	0.0415	0.0188	0.0133	0.0048	-0.0003
	c_3	-0.0379	-0.0780	-0.1156	-0.1244	-0.1368	-0.1430
	c_4	-0.0311	-0.0427	-0.0511	-0.0523	-0.0526	-0.0478
1.9	c_1	-0.0011	-0.0037	-0.0068	-0.0077	-0.0090	-0.0106
	c_2	0.0926	0.0746	0.0534	0.0473	0.0368	0.0237
	c_3	-5.3E-4	-0.0371	-0.0762	-0.0869	-0.1048	-0.1260
	c_4	-0.0205	-0.0325	-0.0438	-0.0465	-0.0506	-0.0541
7.5	c_1	6.8E-5	-0.0018	-0.0011	-0.0012	-0.0015	-0.0013
	c_2	0.1150	0.1115	0.1075	0.1064	0.1044	0.1029
	c_3	0.0649	0.0379	0.0342	0.0301	0.0232	0.0158
	c_4	0.0065	-0.0039	-0.0036	-0.0047	-0.0062	-0.0072
16.9	c_1	-0.0088	-0.0097	-0.0104	-0.0106	-0.0110	-0.0111
	c_2	0.0697	0.0678	0.0657	0.0651	0.0640	0.0637
	c_3	0.0424	0.0328	0.0233	0.0208	0.0166	0.0125
	c_4	0.0047	0.0013	-0.0016	-0.0022	-0.0031	-0.0036
30.0	c_1	-0.0081	-0.0089	-0.0096	-0.0098	-0.0101	-0.0104
	c_2	0.0482	0.0466	0.0450	0.0444	0.0439	0.0434
	c_3	0.0290	0.0220	0.0150	0.0131	0.0103	0.0070
	c_4	0.0029	0.0004	-0.0017	-0.0022	-0.0029	-0.0033

Table 10.2 The t_{df} values when $\theta_0 = 0$ and $WS = 0$.

Wavelength(nm)	380	412	443	490	530	565	673.5	763	868.5
$t_{uf}(0,0)$	0.96356	0.96598	0.96832	0.97104	0.972567	0.97380	0.97763	0.98080	0.98452

$t_{df}(\lambda, \theta_0, WS)$ is interpolated by internal ratio of σ at wind speed (WS). σ is defined by the following equation.

$$\sigma = 0.0731 \cdot \sqrt{WS}$$

Each σ=0.0, 0.1, 0.2, 0.3, 0.4 corresponds to wind speeds WS=0,1.9,7.5,16.9,30 (m/s). t_{df} is calculated at the wavelength closest to the sensor wavelength among these wavelengths.

$t_{df}(\lambda, 0,0)$ is constant. It shows in table 10.2.

10.3 Calculation of Q factor

$Q(\theta', \theta_0, \Delta\phi)$ is expressed as a function of wavelength, chlorophyll a concentration (CHL) , solar zenith angle (θ_0), satellite zenith angle (θ'), relative azimuth angle (Δφ). For calculation of $Q(\theta', \theta_0, \Delta\phi)$), a lookup table (Morel et al., 2002) is used. Look-up tables (DISTRIB_FQ_with_Raman.tar.gz) were obtained over the internet, using anonymous ftp, from oceane.obs-vlfr.fr.

-Wavelength: 412.5, 442.5, 490, 510, 560, 620, 660 nm (7 wavelengths) (MERIS wavelength, SeaDAS uses recent wavelength data)

-CHL: 0.03, 0.1, 0.3, 1.0, 3.0, 10.0 mg / m^3 (6 stages)

The table is expanded on the log 10 scale of CHL (almost equally spaced on log 10)

-Sun zenith angle: 0, 15, 30, 45, 60, 75 ° (6 stages)

-Satellite zenith angle: 1.078, 3.411, 6.289, 9.278, 12.3, 15.33, 18.37, 21.41, 24.45, 27.5, 30.54, 33.59, 36.64, 39.69, 42.73, 45.78, 48.83 ° (17 steps)

-Relative azimuth angle: 0, 15, 30, 45, 60, 75, 90, 105, 120, 135, 150, 165, 180 ° (13 steps)

The $Q(\theta', \theta_0, \Delta\phi)$ coefficient is calculated by four-dimensional linear interpolation of log (CHL), θ 0, θ, Δφ.

$Q(\theta', \theta_0, \Delta\phi)$ is calculated at the wavelength closest to SGLI wavelength among MERIS wavelengths.

11. Ancillary data

Several sets of ancillary data are required for atmospheric correction of SGLI data. We summarize each ancillary data set required below.

11.1 Total ozone

The total ozone concentration (Dobson Units, DU) is required to calculate the ozone optical thickness, and the ozone optical thickness is needed to compute the two-way transmittance of satellite-observed reflectance through the ozone layer. Dobson Units means total ozone concentration at 0 ° C, 1hPa(above mean sea level) and 1 DU is equal to a hundredth of the ozone layer thickness. DU is expressed in mm.

We use OMI (Ozone Monitoring Instrument) or TOVS (Advanced Tiros-N Operational Vertical Sounder) data.

11.2 Sea surface pressure

The atmospheric pressure (hPa) is needed to compute the Rayleigh optical thickness that is required for the computation of ρ_M and the diffuse transmittance of the atmosphere.

We use GGLA objective analysis data. GGLA data are provided by the Japan Meteorological Agency (JMA).

11.3 Sea surface wind

The sea surface wind speed (m/s) and vector(degree) are required for the construction of a sun glint mask. The sea surface wind speed also will be required for estimation of the whitecap reflectance.

We use GGLA objective analysis data. GGLA data are provided by the Japan Meteorological Agency (JMA).

Appendix I　Mean extratrestrial solar irradiance (Thuillier et al.,2003) in consideration with sensor response function.

Table I.1 Mean solar irradiance of GCOM-C/SGLI on Visible and Near-Infrared (VNR)

Band	Telescope	Center wavelength: λ_c [nm]	Solar irradiance: F_0 [W/m^2/μm]
VNR01		379.853	1093.5379
VNR02		412.306	1711.2835
VNR03		443.443	1903.2471
VNR04		489.686	1937.9540
VNR05		529.638	1850.9682
VNR06	Left	565.926	1797.4827
VNR07		672.002	1502.5522
VNR08		672.148	1502.1799
VNR09		762.917	1245.8937
VNR10		866.023	956.2896
VNR11		867.023	956.5311
VNR01		380.030	1092.1436
VNR02		412.514	1712.1531
VNR03		443.240	1898.3185
VNR04		489.849	1938.4602
VNR05		529.640	1850.9604
VNR06	Nadir	566.155	1797.1344
VNR07		671.996	1502.5667
VNR08		672.098	1502.3177
VNR09		763.074	1245.3663
VNR10		866.765	956.2323
VNR11		867.120	956.5352
VNR01		380.212	1090.5931
VNR02		412.589	1712.4760
VNR03		443.051	1893.5879
VNR04		490.311	1941.0715
VNR05	Right	529.664	1851.0657
VNR06		566.377	1796.8275
VNR07		671.950	1502.6962
VNR08		672.120	1502.2582
VNR09		763.234	1244.8290

VNR10	866.713	956.2577
VNR11	867.086	956.5735

Table I.2 Solar Irradiance of GCOM-C/SGLI on Short Wave Infrared (SWI)

Band	Center wavelength: λ_c [nm]	Solar irradiance: F_0 [W/m^2/μm]
SWI01	1054.994	646.5213
SWI02	1385.351	361.2250
SWI03	1634.506	237.5784
SWI04	2209.481	84.2413

SGLI has three telescopes (Left, Nadir and Right).

Appendix II. QA Flags and Masks

Table II.1 QA flag and masks

Bit	Name	Description	Criterion	Mask
0	DATAMISS	No observation data in one or more band[s]		L3
1	LAND	Land pixel		L2
2	ATMFAIL	Atmospheric correction failure		L2
3	CLDICE	Apparent cloud/ice (high reflectance)	ρ_A>0.04	L2
4	CLDAFFCTD	Cloud-affected (near-cloud or thin/sub-pixel cloud)	ρ_A>0.03	L3
5	STRAYLIGHT	Stray light anticipated (ref. L1B stray light flags & image)		
6	HIGLITN	High sun glint predicted (atmospheric corr. abandoned)	$[\rho_G]_N > 0.02$	L2
7	MODGLINT	High sun glint predicted (atmospheric corr. abandoned)	$[\rho_G]_N > 0.005$	L3
8	HIOSOLZ	Solar zenith larger than threshold	$\theta_0 > 70^\circ$	L3
9	HITAUA	Aerosol optical thickness larger than threshold	$\tau_A > 0.5$	L3
10	EPSOUT	Atmospheric correction warning: Epsilon out-of-bounds		
11	OVERITER	Maximum iterations reached for NIR correction		
12	NEGNLW	Negative nLw in one or more bands		L3
13	HIGHWS	Surface wind speed higher than threshold	W/S > 12m/s	
14	TURBIDW	Turbid Case 2 water	*1	
15	SPARE	Spare		

*1) $T_{ind}(869,1630) > th_{low} + \frac{th-th_{low}}{2}$, where th_{low} is 1.4 and th is 1.5.

Appendix III. LUT of Single Scattering Albedo(ω_A) for Aerosol Models

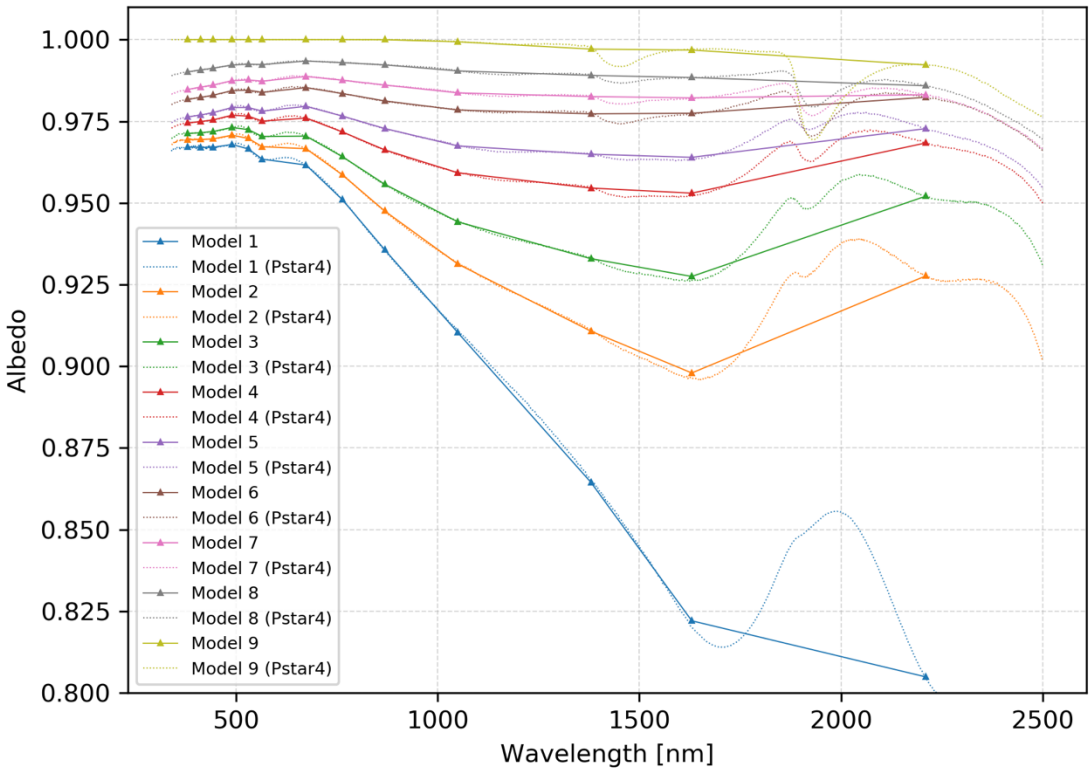

Figure III.1. SSA for each assumed aerosol model. Solid lines represent LUT values which is band weighted averaged. Dash lines represent raw values calculated by Pstar4.

Table III.1. ω_A LUT

Model	VN1	VN2	VN3	VN4	VN5	VN6	VN7	VN9	VN10	SW1	SW2	SW3	SW4
1	0.9672	0.9670	0.9670	0.9679	0.9665	0.9634	0.9616	0.9511	0.9357	0.9103	0.8644	0.8221	0.8049
2	0.9694	0.9694	0.9696	0.9707	0.9698	0.9672	0.9666	0.9586	0.9475	0.9313	0.9107	0.8980	0.9277
3	0.9713	0.9715	0.9719	0.9731	0.9724	0.9703	0.9705	0.9642	0.9557	0.9442	0.9329	0.9275	0.9521
4	0.9745	0.9749	0.9754	0.9768	0.9766	0.9751	0.9760	0.9718	0.9662	0.9592	0.9546	0.9530	0.9684
5	0.9763	0.9769	0.9776	0.9792	0.9792	0.9781	0.9796	0.9766	0.9728	0.9675	0.9649	0.9640	0.9727
6	0.9817	0.9823	0.9830	0.9844	0.9845	0.9839	0.9853	0.9835	0.9812	0.9784	0.9773	0.9775	0.9823
7	0.9847	0.9854	0.9861	0.9874	0.9877	0.9873	0.9887	0.9876	0.9861	0.9837	0.9826	0.9822	0.9831
8	0.9901	0.9907	0.9913	0.9922	0.9925	0.9924	0.9935	0.9930	0.9923	0.9904	0.9890	0.9884	0.9859
8	0.9859	1.0000	1.0000	1.0000	1.0000	1.0000	0.9859	1.0000	1.0000	0.9993	0.9971	0.9968	0.9859

Appendix IV. LUT of Aerosol Extinction Coefficient (K_{ext}) for Aerosol Models

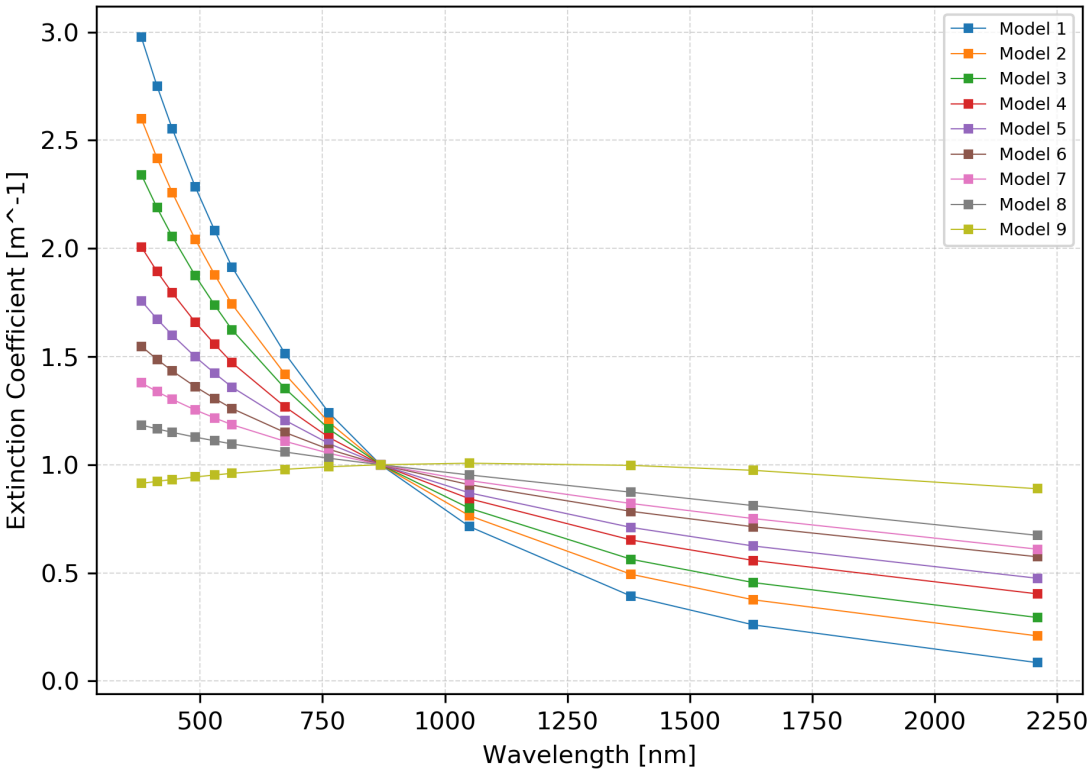

Figure IV.1. K_{ext} values normalized by K_{ext} at VN10 for each assumed aerosol model. Solid lines represent LUT values which is band weighted averaged.

Table IV.1. K_{ext} LUT

Model	VN1	VN2	VN3	VN4	VN5	VN6	VN7	VN9	VN10	SW1	SW2	SW3	SW4
1	2.976	2.750	2.554	2.285	2.081	1.914	1.514	1.240	1.000	0.714	0.393	0.260	0.085
2	2.599	2.417	2.259	2.042	1.877	1.742	1.418	1.196	1.000	0.764	0.494	0.376	0.209
3	2.340	2.188	2.056	1.874	1.737	1.624	1.352	1.166	1.000	0.799	0.563	0.455	0.294
4	2.007	1.893	1.795	1.659	1.556	1.472	1.268	1.126	1.000	0.843	0.652	0.558	0.403
5	1.758	1.674	1.600	1.499	1.422	1.359	1.205	1.098	1.000	0.870	0.710	0.624	0.475
6	1.548	1.487	1.434	1.361	1.306	1.260	1.149	1.071	1.000	0.908	0.785	0.713	0.575
7	1.379	1.338	1.303	1.253	1.216	1.185	1.108	1.053	1.000	0.927	0.821	0.751	0.610
8	1.184	1.166	1.150	1.128	1.111	1.096	1.059	1.030	1.000	0.953	0.873	0.811	0.674
8	0.914	0.923	0.932	0.944	0.953	0.961	0.979	0.991	1.000	1.007	0.997	0.974	0.889

Appendix V LUT of Aerosol Scattering Phase Function (P_A) for Assumed Aerosol Models

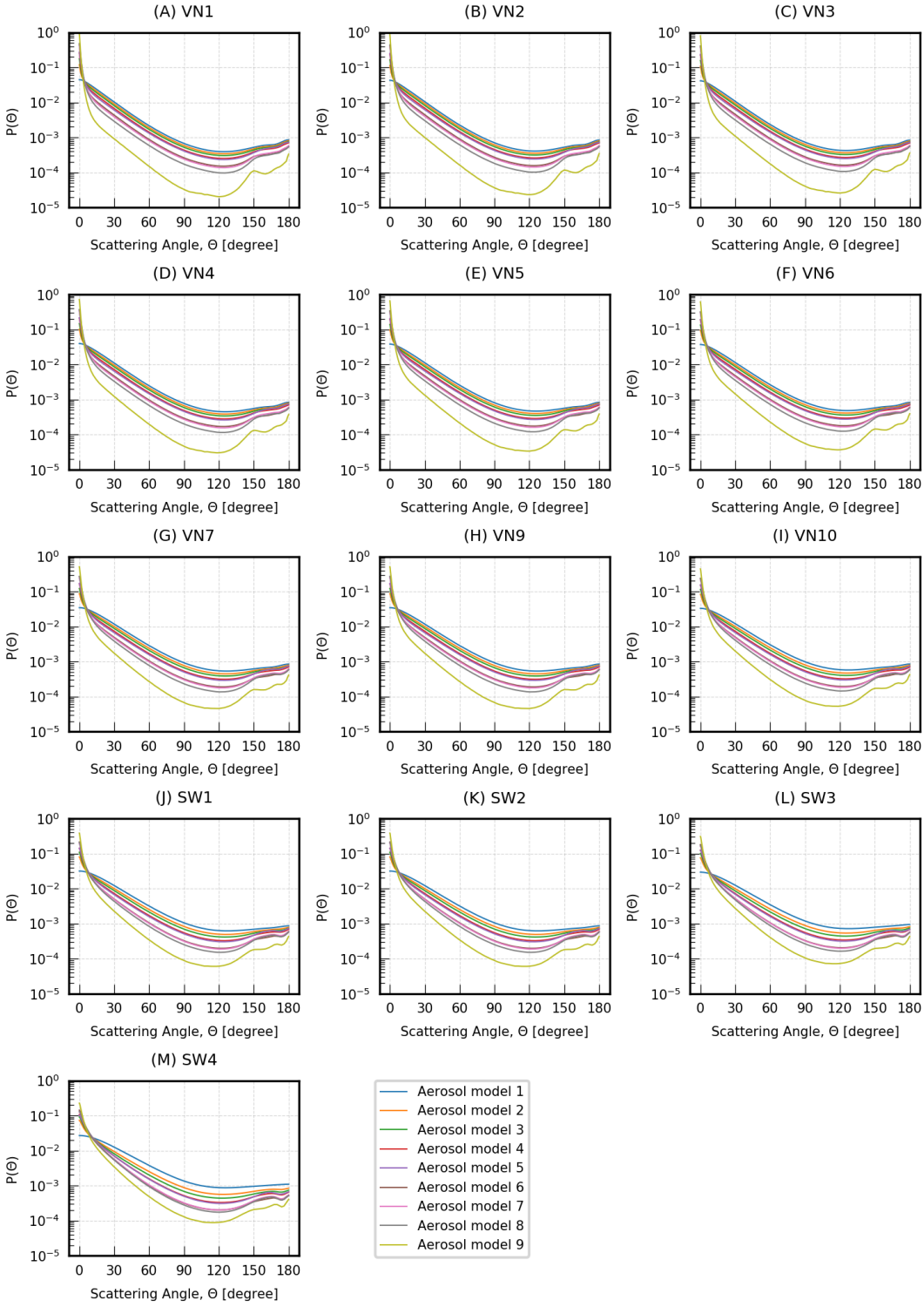

Figure V.1. P_A values for each assumed aerosol model.

References

Bodhaine, Barry A., Norman B. Wood, Ellsworth G. Dutton, James R. Slusser, 1999: On Rayleigh Optical Depth Calculations. *J. Atmos. Oceanic Technol.*, **16**, 1854–1861. doi: 10.1175/1520-0426(1999)016<1854:ORODC>2.0.CO;2

Ding K. and H. R. Gordon (1995), Analysis of the influence of O2 A-band absorption on atmospheric correction of ocean color
imagery, APPLIED OPTICS, Vol. 34, No. 12, pp.2068-2080.

Frouin R., M. Schwindling and P.-Y. Deschamps (1996), Spectral reflectance of sea foam in the visible and near-infrared: In situ measurements and remote sensing implications, *J. GEOPHYSICAL RESEARCH*, VOL. 101, NO. C6, PAGES 14,361-14,371.

Fukushima H., A. Higurashi, Y. Mitomi, T. Nakajima, T. Noguchi, T. Tanaka and M. Toratani (1998), Correction of atmospheric effect on ADEOS/OCTS ocean color data: Algorithm description and evaluation of its performance, Journal of Oceanography, Vol.54, pp.417-430.

Gordon and M. Wang (1994), Retrieval of water-leaving radiance and aerosol optical thickness over the oceans with SeaWIFS: a preliminary algorithm , Applied Optics, 33, 443–452.

Han L. (1997): Spectral reflectance with varying suspended sediment concentrations in clear and algae-laden waters, Photogram. Engineering & Remote Sensing, 63, 701-705.

Morel, A. and B. Gentili, 1996: Diffuse reflectance of oceanic waters. III. Implication of bidirectionality for the remote sensing problem. *Appl. Opt.*, Vol. **35:** 4850-4862.

Morel A., D. Antoine, and B. Gentili (2002), Bidirectional reflectance of oceanic waters: acconting for Raman emission and varying particle scattering phase function, Appl. Opt.,Vol.41, No..30, pp.6289-6306.

Mueller J. L., A. Morel, R. Frouin, C. Davis, R. Arnone, K. Carder, Z. P. Lee, R. G. Steward, S. Hooker, B. Holben, C. D. Mobley, S. McLean, M. Miller, C. Peitras, G. S. Fargion, K. D. Knoblspiesse, J. Porter and K. Boss (2003), Ocean Optics Protocols For

Satellite Ocean Color Sensor Validation, Revision 4, Volume III:Radiometric Measurements and Data Analysis Protocols, CHAPTER 4, NASA/TM-2003-21621, Rev-Vol III, pp.32-59.

Stramska, M. and T. Petelski (2003), Observations of oceanic whitecaps in the north polar waters of the Atlantic, J. Geophys. Res., 108C3, 3086. doi: 10.1029/2002JC001321

Thuillier, G., M. Hersé, D.Labs, T. Foujols and W. Petermans.(2003), The Solar Spectral Inradiance from 200 to 2400 nm as Measured by the Solspec Spectrometer from the Atlas and Eureca Missions, Solar Physics, 214 (1): 1-22.

Mitsuhiro Toratani, Hajime Fukushima, Hiroshi Murakami and Akihiko Tanaka (2007), Atmospheric correction scheme for GLI with absorptive aerosol correction, Journal of Oceanography, Vol.63, pp. 525-532.

Voigt S., J. Orphal, and J. P. Burrows (1999), High-Resolution Reference Data by UV-Visible Fourier-Transform Spectroscopy: 1. Absorption Cross-Sections of NO_2 in the 250-800 nm Range at Atmospheric Temperatures (223-293 K) and Pressures (100-1000 mbar), Chemical Physics Letters, in preparation

Voigt S., J. Orphal, K. Bogumil, and J. P. Burrows (2001), "The Temperature Dependence (203-293 K) of the Absorption Cross-Sections of O3 in the 230–850 nm region Measured by Fourier-Transform Spectros-copy", *Journal of Photochemistry and Photobiology A: Chemistry*, **143**, 1–9.

Wang M.(2006), Effects of ocean surface reflectance variation with solar elevation on normalized water-leaving radiance, Applied Optics, Vol.45, No.17, pp.4122-4128.